# Combined ultrasound and photoacoustic imaging to detect and stage deep vein thrombosis: phantom and *ex vivo* studies

**Andrei B. Karpiouk**
University of Texas at Austin
Department of Biomedical Engineering
Austin, Texas 78712

**Salavat R. Aglyamov**
University of Texas at Austin
Department of Biomedical Engineering
Austin, Texas 78712
    and
Russian Academy of Sciences
Institute of Mathematical Problems of Biology
Pushchino, Moscow Region, 142290
Russia

**Srivalleesha Mallidi**
**Jignesh Shah**
University of Texas at Austin
Department of Biomedical Engineering
Austin, Texas 78712

**W. Guy Scott**
WinProbe Corporation
North Palm Beach
Florida 33408

**Jonathan M. Rubin**
University of Michigan
Department of Radiology
Ann Arbor, Michigan 48109

**Stanislav Y. Emelianov**
University of Texas at Austin
Department of Biomedical Engineering
Austin, Texas 78712

**Abstract.** Treatment of deep venous thrombosis (DVT)—a primary cause of potentially fatal pulmonary embolism (PE)—depends on the age of the thrombus. The existing clinical imaging methods are capable of visualizing a thrombus but cannot determine the age of the blood clot. Therefore, there is a need for an imaging technique to reliably diagnose and adequately stage DVT. To stage DVT (i.e., to determine the age of the thrombus, and therefore, to differentiate acute from chronic DVT), we explored photoacoustic imaging, a technique capable of noninvasive measurements of the optical absorption in tissue. Indeed, optical absorption of the blood clot changes with age, since maturation of DVT is associated with significant cellular and molecular reorganization. The ultrasound and photoacoustic imaging studies were performed using DVT-mimicking phantoms and phantoms with embedded acute and chronic thrombi obtained from an animal model of DVT. The location and structure of the clots were visualized using ultrasound imaging, while the composition, and therefore age, of thrombi were related to the magnitude and spatiotemporal characteristics of the photoacoustic signal. Overall, the results of our study suggest that combined ultrasound and photoacoustic imaging of thrombi may be capable of simultaneous detection and staging of DVT. © *2008 Society of Photo-Optical Instrumentation Engineers.*
[DOI: 10.1117/1.2992175]

## 1 Introduction

Most clinically important pulmonary emboli (PE) originate from a proximal deep vein thrombosis (DVT) of a leg (popliteal, femoral, or iliac veins). An estimated annual incidence of a venous thromboembolism (a spectrum of conditions including DVT and PE) in the United States is more than 250,000 people, and more than 100,000 patients die annually from PE.[1,2] Most often PE is related to DVT, where a part of the thrombi breaks free, travels through veins, and reaches lungs.[3] To detect a DVT, venous ultrasonography is employed clinically.[4–8] This method is based on a combination of gray-scale imaging, color-flow Doppler, and compression ultrasound imaging of a vein and a nearby artery while an external pressure is being applied. As an alternative, contrast venography can be used. The contrast agent is injected in a vein below the clot and x-ray imaging of the vein shows how DVT blocks contrast agent proliferation along the vein.[9–12] Finally, magnetic resonance imaging (MRI) can detect thrombosis in veins.[13–16] MRI has similar sensitivity as the ultrasonography, although it is expensive, not portable, and often requires contrast agents to be injected.[17]

All these clinical and investigational imaging methods are successful in detecting DVT but cannot distinguish between old and new clots. However, the treatment of a deep venous thrombosis depends on the age of DVT.[18] The main treatment

Address all Correspondence to: Stanislav Emelianov, 1 University Station C0800, Austin, TX 78712; Tel: 512-471-1733; Fax: 512-471-0616; Email: emelian@mail.utexas.edu

goals for DVT are to stop the further formation of the clot and to prevent the recurrence of a thrombus following a PE occurrence. For acute thrombi, heparin, a powerful injected anticoagulant, is used in spite of significant bleeding risks.[19] In contrast, heparin is not required for chronic thrombi, which are, at most, treated with coumadin, a less potent, oral anticoagulant.[18] Therefore, there is a clinical need for a technique that is widely available, simple to perform, safe, and can reliably diagnose and adequately stage DVT.

Maturation of DVT is associated with the reorganization of the blood clot. An acute clot, formed in a relatively static environment, tends to contain more enmeshed erythrocytes, and is therefore known as a red or stasis thrombus. As the blood clot matures, it is typically firmly adherent to a vessel wall and becomes gray-white-yellow,[20] composed of a tangled mesh of platelets, fibrins, and degenerating leukocytes. Such reorganization of the clot may result in decreased hemoglobin concentration within the clot, and therefore, reduced optical absorption of DVT. Consequently, photoacoustic imaging—an imaging technique capable of noninvasive measurements of optical absorption of tissue—could be used to stage the detected thrombi.

The photo/opto/thermoacoustic effect relies on absorption of a short pulse of an electromagnetic radiation, and a subsequent emission of a thermoelastic acoustic wave.[21,22] Specifically, a pulsed laser radiation with a wavelength tuned to absorption of red blood cells (RBCs) is used as a source of the electromagnetic radiation. Due to a strong optical absorption, the acute blood clot should potentially emit a stronger photoacoustic signal compared to that of the chronic DVT.

In this work, the photoacoustic imaging of DVT is initially explored. Using a high-frequency single-element focused ultrasound transducer and pulsed laser, the photoacoustic and ultrasound images were acquired simultaneously. Two cylindrical samples of poly(vinyl) alcohol (PVA) with different concentrations of RBC solution were used to model the acute and chronic thrombi. The ultrasound images were used to visualize the structure of the thrombi. The differences in magnitudes of photoacoustic radio-frequency (rf) signals were used to differentiate acute and chronic clots. The developed approach was also evaluated using phantoms with embedded chronic and acute thrombi obtained from an animal model of DVT.[20,23] Overall, our studies suggest that the combined photoacoustic and ultrasound imaging is a candidate approach for detection and staging of DVT.

## 2 Materials and Methods

### 2.1 Phantoms and Ex Vivo Tissue Samples

The experiments were first performed using tissue-mimicking phantoms with models of acute and chronic DVT. A 6.37-mm-diam tube (WLS25275-BC, Sargent-Welch, Incorporated, Buffalo, New York) was used to mimic a vessel wall. This artificial vein was attached to a fixture and then embedded into 100-×50-×45-mm (L×W×H) rectangular block made out of 10% weight concentration of gelatin (type A, Sigma-Aldrich, Saint Louis, Missouri). To produce a background material with similar optical and ultrasonic properties of soft tissues, a 20% volume concentration of fat-free milk was added to elevate optical scattering,[24,25] and 0.8% weight concentration of 40-$\mu$m silica particles[26] (Sigma-Aldrich)
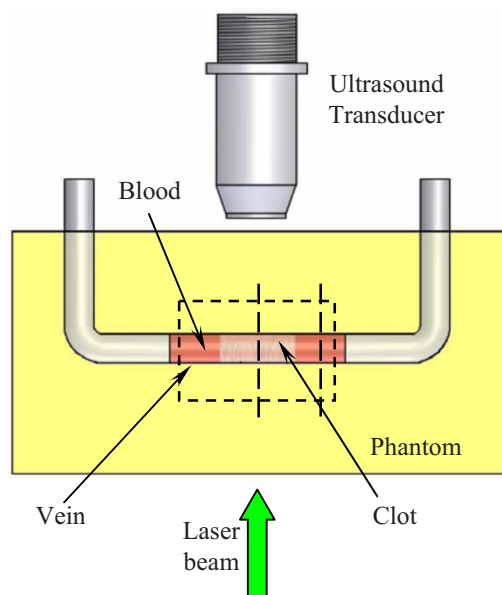


**Fig. 1** Diagram of a phantom and an experimental setup used in ultrasound and photoacoustic imaging of DVT. The dashed rectangle schematically represents the imaging area, and the vertical lines indicate the positions of the photoacoustic signals used for quantitative comparison of different clots.

was added for ultrasonic backscattering. The light absorption and reduced scattering coefficients of this gelatin were estimated to be $0.09 \pm 0.01$ cm$^{-1}$ and $5.82 \pm 0.04$ cm$^{-1}$, respectively (mean ± standard deviation).

Venous blood was modeled by a solution of heparinized human RBCs obtained from a local blood and tissue center. The RBCs were 50% diluted in saline to match the normal concentration of RBC in the whole human blood. The light extinction coefficient, measured in a thin layer of this solution, was $293 \pm 9$ cm$^{-1}$.

The 13- to 20-mm-long and 6.4-mm-diam artificial clots were constructed using 7% weight concentration of PVA (Celvol 165SF, Celanese, Dallas, Texas). A 2% weight concentration of 40-$\mu$m silica particles was added in all artificial clots for ultrasound scattering, while PVA by itself is already a light scattering material. The light absorption and reduced light scattering coefficients were estimated to be $0.4 \pm 0.3$ cm$^{-1}$ and $6.8 \pm 0.3$ cm$^{-1}$, respectively. These values are similar to those reported in the literature.[27] To position the clots reliably in the vein and to avoid the penetration of the RBC solution between the clot and the vessel wall, the diameter of the clot was slightly larger than the diameter of the dialysis tubing. To model acute clots, a base RBC solution, was added in PVA, and pure saline with no RBCs was used in artificial chronic clots. The light absorption coefficient of an acute clot was estimated to be 9% lower than that of RBC solution, since both PVA and silica particles have negligible optical absorption coefficients in comparison with RBC solution. The clot-containing vein was embedded in a gelatin phantom, as shown in Fig. 1. The remaining part of the vessel was filled with the 50% RBC solution representing venous blood.

The combined ultrasound and photoacoustic imaging were also explored to image acute and chronic thrombi obtained from a well established small animal model of stasis-induced venous thrombosis,[23] which closely reproduces thrombus development in clinical disease. Sprague-Dawley rats underwent surgery to initiate thrombus formation in the inferior vena cava, and 3-day-old (acute thrombus) and 9-day-old (chronic thrombus) clots were surgically removed from the animals. The thrombi were then positioned in a gelatin phantom at 15 mm depth and 13 mm apart from each other and imaged *ex vivo*. The diameters of the acute and chronic thrombi in the imaging plane were approximately 2 and 3.5 mm, respectively.

## 2.2 Imaging System

The combined ultrasound and photoacoustic imaging system is schematically shown in Fig. 1. During the experiments, the phantoms were placed in a water cuvette with an optical window at the bottom to allow laser light to enter from underneath (Fig. 1). The phantoms were irradiated with 5-ns pulses using a Q-switched Nd:YAG laser (Polaris II, New Wave Research, Freemont, California) operating at 532-nm wavelength. A focused, single element ultrasound transducer (Panametrics-NDT, Waltham, Massachusetts) with a center frequency of 7.5 MHz, a fractional bandwidth of 60%, an aperture of 12.7 mm, and an f/number of 4 was positioned on the opposite side of the phantom. Assuming the speed of sound of 1500 m/s, the ultrasound images obtained using this transducer should have 170-$\mu$m axial (i.e., along the ultrasound beam) and 800-$\mu$m lateral (i.e., across the beam) resolutions, respectively. During the imaging, both the ultrasound transducer and the laser beam were simultaneously moved by 200 $\mu$m in the horizontal direction using a computer controlled, high-precision positioning system (model MN10-0050-M02-21, Velmex, Bloomfield, New York). Using the same transducer, both photoacoustic and ultrasound signals were acquired by the 12-bit, 50-MHz bandwidth, 100-MS/s digitizer (CompuScope 12100, GaGe Applied, Lockport, Illinois). Overall, all components of the imaging system including the pulsed laser, an ultrasound pulser/receiver (model 5910PR, Panametrics-NDT), the motion controller (nuDrive, National Instruments, Austin, Texas) and the digitizer were interfaced and controlled using a developed software interface written in LabVIEW.

## 2.3 Data Acquisition and Signal/Image Processing

The dependence of a photoacoustic signal magnitude on a concentration of the RBC solution was measured using the phantom with an embedded modeled vein filled with RBC solution. For each concentration, the photoacoustic measurements were performed with laser pulses of different (9 to 23 mJ) energy levels, and then normalized. The baseline signal was estimated using a vein filled with saline.

The imaging of the tissue-mimicking phantoms with modeled thrombi was performed along the coronal cross section of the vessel, as shown in Fig. 1. To qualitatively and quantitatively compare the acute and chronic thrombi obtained from the rat model of DVT, the transverse cross sections were imaged within one scan. In all imaging experiments, an average of more than ten laser pulses was applied at each lateral po-
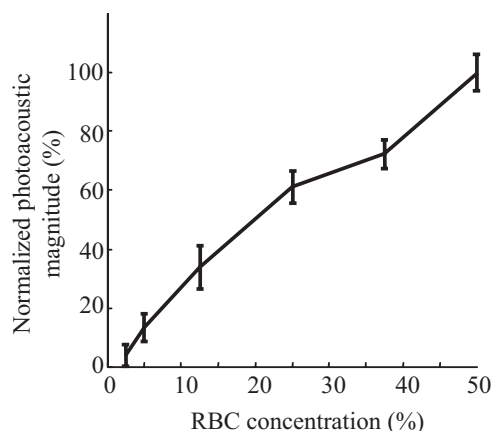


**Fig. 2** Dependence of normalized magnitude (mean value ± standard deviation) of the photoacoustic pressure transient on volume concentration of RBC solution in saline. RBC concentration of 50% corresponds to a concentration of RBC solution in normal human blood.

sition to reduce the pulse-to-pulse laser energy variations. The corresponding photoacoustic signals, followed by ultrasound signals, were acquired and stored for off-line processing. Due to a weak light absorption in chronic clots, these clots were imaged with high (23 mJ) laser energy, while the phantom with an artificial acute clot was imaged using low (9 mJ) laser pulses.

The captured photoacoustic and ultrasound rf signals were averaged, demodulated, and scan converted to cover the desired region of interest, pictorially shown in Fig. 1. In addition, the magnitude of the photoacoustic signal was corrected for the exponential (Beer's law) losses of optical fluence with depth. Both ultrasound and photoacoustic images were formed using the magnitude of the basebanded signal. No sophisticated reconstruction techniques were applied to produce photoacoustic images. For quantitative comparison, the photoacoustic signals from clots and blood-filled veins were analyzed (the positions of the rf lines are shown in Fig. 1). Finally, the maximum of each photoacoustic rf signal within the region of interest was estimated and plotted as a function of the lateral position. No compensation for the optical fluence was applied to calculate these photoacoustic profiles or to quantitatively compare photoacoustic rf signals.

## 3 Results

### 3.1 Phantom Studies

The dependence of the magnitude of the photoacoustic signal on the concentration of the RBC solution is shown in Fig. 2. As expected, the dependence is monotonic and a higher concentration of RBC solution produces a higher photoacoustic response. Therefore, an acute clot with a higher concentration of RBC should produce a greater photoacoustic response compared to a chronic clot with lower concentration of RBC.

The ultrasound and photoacoustic images of the phantoms with the artificial clots are presented in Fig. 3. Specifically, images of the acute and chronic clots in the vein filled with blood are presented in Figs. 3(a) and 3(b), and Figs. 3(c) and 3(d), correspondingly. The chronic clot inside the vein filled with saline solution is presented in Figs. 3(e) and 3(f).
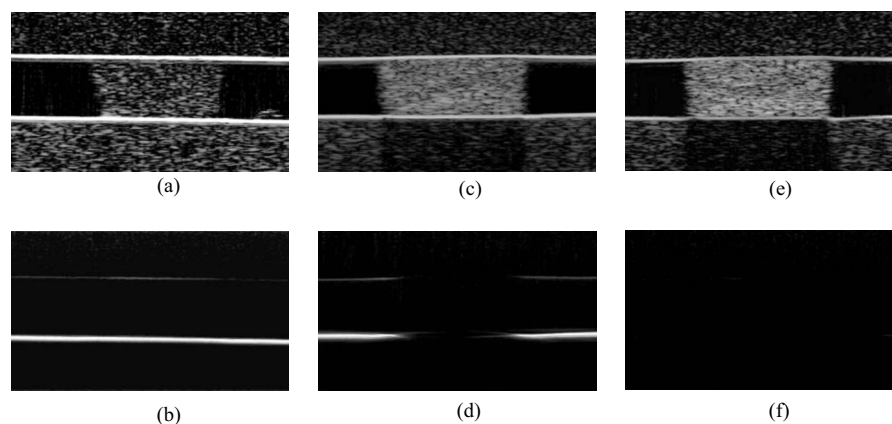
**Fig. 3** (a), (c), and (e) The ultrasound and (b), (d), and (f) photoacoustic images depict the coronal views of the phantoms with artificial clots inside of the modeled veins and background tissue. All images are 30.4×18.0 mm. The acute and chronic clots in the vein filled with blood are presented in (a) and (b), and (c) and (d), correspondingly. The chronic clot inside the vein filled with saline solution is presented in (e) and (f). The compensation for exponential decay of optical fluence with depth was applied to all photoacoustic images.

In ultrasound images [Figs. 3(a), 3(c), and 3(e)], the structural features of all phantoms such as background tissue, vessel walls and blood clot are clearly depicted. These B-scans are slightly different due to the differences between the phantoms and the imaging planes. As expected, acute clots cannot be differentiated from chronic clots in ultrasound images. The acute clot in Fig. 3(a) appears darker than the chronic clots in Figs. 3(c) and 3(e) and does not produce an ultrasound shadow. However, these differences are more likely attributed to a slight off-center position of the imaging plane where the variations of the phantom material along the vein result in a different refraction of the ultrasound waves from the boundaries. Indeed, the acute clot and the background tissue in Fig. 3(a) appear to be similar, although no RBCs were added in the background material.

The photoacoustic image of the phantom with an acute clot is shown in Fig. 3(b). Using the band-limited ultrasound transducer, the photoacoustic response from an object with relatively uniform distribution of optical absorption coefficient will be represented by two signals corresponding to the boundaries of the vessel or the blood clot.[28,29] Furthermore, the lower boundary exposed to a greater light intensity (or fluence) will exhibit a larger photoacoustic response generated in the acute clot and the lumen of the vessel. However, since the concentrations of RBC in acute clot and venous blood are nearly the same, the photoacoustic imaging cannot differentiate between acute clot and luminal blood.

The photoacoustic image of the phantom with a chronic clot is shown in Fig. 3(d). As expected, the photoacoustic response from the luminal blood is relatively high. However, the magnitude of the photoacoustic signal from the chronic clot is reduced. This is due to almost no optical absorption in the chronic clot. This effect cannot be explained by additional ultrasound attenuation, which produces ultrasound shadow in Figs. 3(c) and 3(e). Brightness of the chronic clots near upper and lower tissue-clot interfaces is similar, thus indicating low attenuation of ultrasound. The upper clot-tissue interface in the area of thrombus is no longer visible, although it was exposed to the higher laser energy again indicating the weak optical absorption of the clot compared with RBC solution.

Overall, a chronic clot produces relatively small photoacoustic response in comparison with acute thrombi or luminal blood.

Compared to RBCs, the other materials of the phantom such as PVA, gelatin, and dialysis tubing do not significantly absorb light at this wavelength, and therefore do not generate photoacoustic transients—it is demonstrated by photoacoustic imaging of a phantom with a chronic clot and without the RBC solution in the lumen of the vessel [Fig. 3(f)]. Indeed, the photoacoustic image is nearly featureless, indicating the modest optical absorption coefficient in the phantom at the given wavelength.

The photoacoustic rf signals generated in the acute and chronic clots and in RBC/saline solution are quantitatively contrasted in Fig. 4. The transducer is located closer to the origin of the plot, while the laser irradiation is directed from an opposite side (see also Fig. 1).

The photoacoustic rf signals from the acute clot [Fig. 4(a)] and from the vein with RBC solution [Figs. 4(b) and 4(d)] consist of two peaks corresponding to the boundaries of optical absorbers. Due to the strong optical absorption of the acute clot and venous blood, and given the orientation of laser irradiation, the magnitude of the photoacoustic signals from the upper tissue-vein interface (located at 5.5 mm) is significantly lower than the magnitude of peaks corresponding to the rf signal from lower tissue-vein interface (located at 12 mm). The magnitudes of photoacoustic rf signals from the chronic clots [Figs. 4(c) and 4(e)] and from the vein with saline [Fig. 4(f)] are significantly lower in comparison with both the acute clot [Fig. 4(a)] and the RBC solution [Figs. 4(b) and 4(d)]. The signal from the upper tissue-vein interface in the area of the chronic clot is not noticeable due to insignificant light absorption.

To further underline the differences in the photoacoustic signals from the acute and chronic clots, the photoacoustic profiles obtained from the images in Figs. 3(b), 3(d), and 3(f) are plotted in Fig. 5. The photoacoustic profile for the chronic clot in the vein filled with saline has low magnitude and does not vary with lateral position, i.e., the chronic clot cannot be
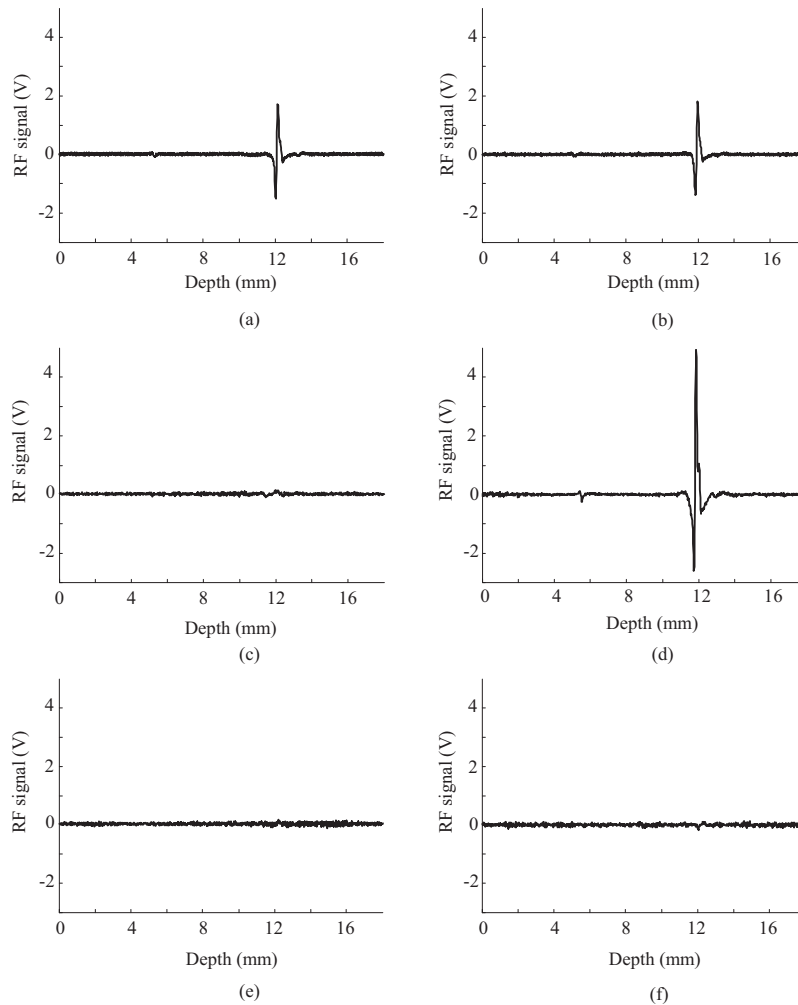
**Fig. 4** The photoacoustic rf signals from the phantoms with (a) and (b) the artificial acute and (c) and (d) chronic thrombi and RBC solution in the lumen, and the phantom with chronic clot and saline in the vein [(e) and (f)]. The photoacoustic rf signals taken along the vertical line passing through the clots are presented in (a), (c), and (d). The rf signals recorded from the vessel with no clots are presented in (b), (d), and (f).

distinguished from the background. The phantom with the acute clot also exhibits a nearly uniform photoacoustic profile, but the magnitude is high. The photoacoustic signal in the area of the acute clot itself is slightly lower because approximately 9% of RBCs were replaced by PVA and silica particles, thus reducing the optical absorption in acute clot in comparison with venous blood. On the contrary, the magnitude of the photoacoustic profile of the phantom with chronic clot is low in the region of the clot itself, while the photoacoustic signal from the vein filled by the RBC solution is considerably higher.

### 3.2 *Ex Vivo Studies*

The photoacoustic and ultrasound imaging of DVT was further evaluated using thrombi obtained from a rat model of DVT. The ultrasound and photoacoustic images of chronic (9-day-old) and acute (3-day-old) thrombi are shown in Fig. 6. The boundary between two layers of the gelatin is clearly visible in the ultrasound image [Fig. 6(a)] due to a slight mismatch in acoustic impedances. This boundary, however, is not visible on the photoacoustic image [Fig. 6(b)], since there are no differences in optical absorption between these two
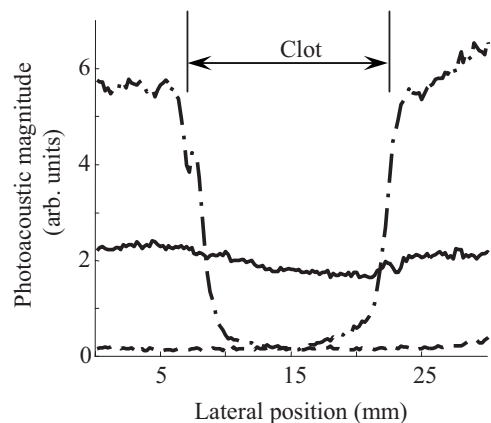
**Fig. 5** The photoacoustic profiles estimated in the phantoms with the acute (solid line) and chronic (dot-dashed line) clots and blood-filled vein, and the phantom with the chronic clot and saline solution in the lumen (dashed line).
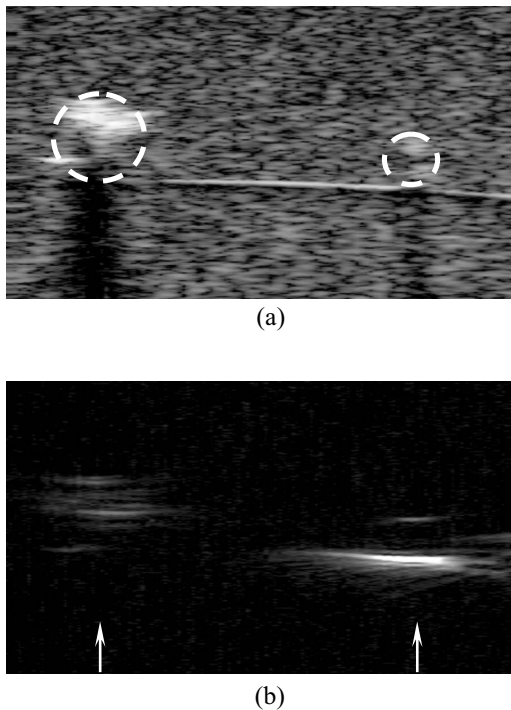
(a)



(b)

**Fig. 6** The (a) ultrasound and (b) photoacoustic images representing the cross sectional view of the chronic, 9-day-old (left) and acute 3-day-old (right) clots embedded in the gelatin phantom. The thrombi were obtained from a rat model of stasis-induced DVT. Both images are $22 \times 13$ mm. The locations and sizes of both clots in the ultrasound image are denoted by dashed circles.

layers. This fact again demonstrates that the contrast mechanisms in ultrasound and photoacoustic images are not related. The differences in ultrasound appearance of both clots may be attributed to the difference of both the thrombi sizes and content.[30] The photoacoustic image of the acute thrombus consists of two transient pressure waves from the boundaries of the clot. The lower clot-tissue interface generates a higher signal than the upper interface. These features of the photoacoustic response are very similar to those of the artificial acute clot shown in Fig. 3(b). In contrast, the chronic clot appears darker and is represented by the several transient pressure waves.

The photoacoustic rf signals generated in the chronic and acute thrombi are shown in Fig. 7. The rf signal from the acute clot [Fig. 7(a)] closely resembles the rf signal from the artificial clot [Fig. 4(a)]. Again, the magnitude of the transient pressure from the lower clot-tissue interface is higher than the magnitude of the wave from the upper interface. However, both waves are clearly noticeable because higher laser energy reached the upper boundary of the smaller ($\sim$2 mm diam) acute clot compared with the artificial 6.4-mm-diam acute clot. The overall magnitude of the rf signal from the chronic clot is lower compared with the acute clot, indicating lower optical absorption of chronic DVT. However, the noticeable transient pressures generated within the chronic clot suggest a heterogeneous structure of the clot, and therefore a variation of light absorption coefficient inside the clot.

The differences between chronic and acute thrombi are further demonstrated in the photoacoustic profile shown in
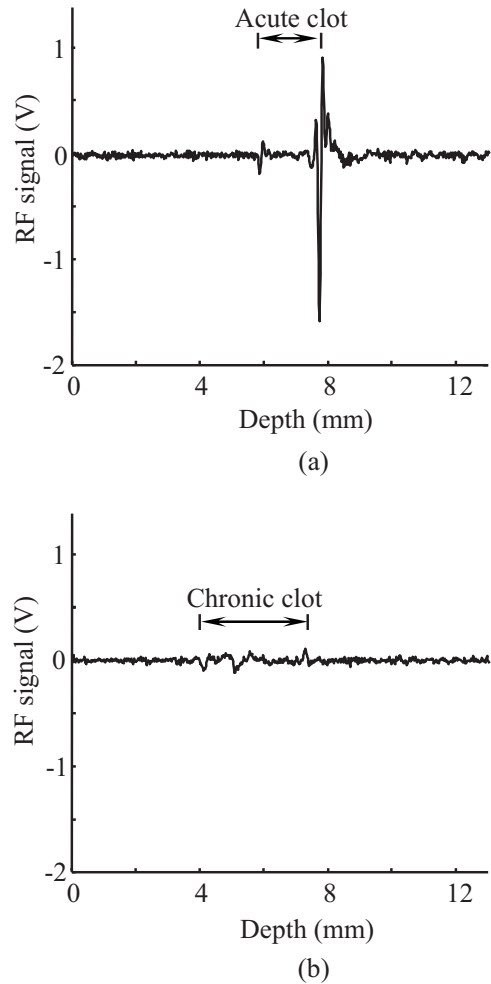


(a)



(b)

**Fig. 7** The photoacoustic rf signals from the phantom with (a) acute and (b) chronic animal thrombi taken along the vertical lines indicated by arrows in Fig. 6(b).

Fig. 8. As expected, the magnitude of the photoacoustic response from the acute clot is greater than from the chronic clot. The photoacoustic signal from the chronic clot is slightly greater than the background level of the photoacoustic response. It is clear that the older clot is characterized by a weaker photoacoustic signal.

## 4 Discussion and Conclusions

The magnitude of a photoacoustic signal generated in RBC solution depends monotonically on the RBC concentration—a higher concentration of RBCs results is a greater photoacoustic signal. Since the fraction of RBCs in thrombi decreases as the blood clot ages, the magnitude of the photoacoustic signal from the thrombus is inversely proportional to the age of the clot.

As evident from the photoacoustic profiles shown in Figs. 5(b) and 5(d), the energy of the laser pulse (or optical fluence) affects the magnitude of a photoacoustic signal. Therefore, it is not the absolute but relative photoacoustic measurements that may be needed to differentiate acute and chronic clots. For example, the blood next to the clot can be used to determine the age of the thrombi. If the thrombus is too long and
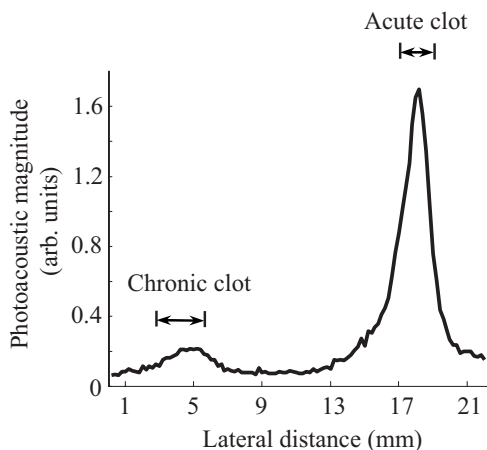
**Fig. 8** The profile of the photoacoustic signals for the chronic (9-day-old) and acute (3-day-old) clots.

measuring the photoacoustic signal from the blood near the clot is not possible, or if significant changes of optical properties of soft tissues along the vein are expected, then a nearby artery can be used as a baseline measurement. The difference in oxygenation levels of blood in the vein and in the artery will not affect the accuracy of measurements if the optical wavelength is carefully chosen.[31]

In our experiments, a 532-nm pulsed laser source was used, since the focus of the current study was to demonstrate the feasibility of a photoacoustic technique to stage DVT, i.e., to differentiate acute blood clots from chronic DVT. This wavelength is not optimal, as the light attenuation in soft tissues is very high.[32] In clinical applications, wavelengths within 750 to 950 nm should be used because the penetration depth of light is reasonable in this spectral range. Several pulsed laser systems including Alexandrite (760 nm), Ti:Sapphire (890 nm), tunable and dye lasers operate in this near-infrared spectral range. Correct and accurate choice of the laser irradiation conditions together with appropriate ultrasound techniques could be used for up to 70-mm imaging depth without noticeable loss of resolution.[33] The femoral vein is usually located 15 to 20 mm away from the skin.[34] In addition, pressure can be applied to deform soft tissues, thus decreasing the distance between the skin and DVT. Deformations can also be used to combine the ultrasound and photoacoustic imaging with elasticity imaging.[20,35] This integrated multimodal imaging technique[36] can provide the desired structural and functional information needed for the detection, diagnosis, and staging of DVT.

For clinical studies, a real-time ultrasound and photoacoustic imaging system will be required. Such a system can be based on a typical ultrasound imaging system interfaced with a pulsed laser source. For grayscale ultrasound imaging, an array of transducer elements will be used both to transmit the ultrasound pulses and to receive the backscattered ultrasound signals. In addition, Doppler and power/color flow imaging will be used to confirm the presence of the DVT. In photoacoustic imaging, a laser pulse will be transmitted into the tissue using a fiber optic delivery system integrated with the ultrasound probe, i.e., laser irradiation will be delivered from the same side where the ultrasound transducer is located. The

photoacoustic signal will be detected by the same ultrasound transducer and electronics used for ultrasound imaging.

In summary, the experimental phantom and *ex vivo* tissue studies are performed to initially test the hypothesis that photoacoustic imaging, augmented by ultrasound imaging, can differentiate acute and chronic DVTs. The analysis of photoacoustic signal magnitude and spatiotemporal characteristics of the photoacoustic images suggests that acute and chronic clots can be differentiated by photoacoustic imaging. Overall, the combined ultrasound and photoacoustic imaging of blood clots has the potential to become an effective imaging method to diagnose DVT.

### References

1. P. Augustinos and K. Ouriel, "Invasive approaches to treatment of venous thromboembolism," *Circulation* **110**, I-27–I-34 (2004).
2. S. J. McRae and J. S. Ginsberg, "Initial treatment of venous thromboembolism," *Circulation* **110**, I-3–I-9 (2004).
3. J. Hirsh and J. Hoak, "Management of deep vein thrombosis and pulmonary embolism," *Circulation* **93**, 2212–2245 (1996).
4. D. Scarvelis and P. S. Wells, "Diagnosis and treatment of deep-vein thrombosis," *Can. Med. Assoc. J.* **175**, 1087–1092 (2006).
5. B. K. Zierler, "Ultrasonography and diagnosis of venous thromboembolism," *Circulation* **109**, 9–14 (2004).
6. O. Ozbudak, I. Erogulları, C. Ogus, A. Cilli, M. Turkay, and T. Ozdemir, "Doppler ultrasonography versus venography in the detection of deep vein thrombosis in patients with pulmonary embolism," *J. Thromb. Thrombolysis* **21**, 159–162 (2006).
7. A. Cogo, A. W. A. Lensing, M. M. W. Koopman, F. Piovella, S. Siragusa, P. S. Wells, S. Villalta, H. R. Büller, A. G. G. Turpie, and P. Prandoni, "Compression ultrasonography for diagnostic management of patients with clinically suspected deep vein thrombosis: prospective cohort study," *Br. Med. J. (Clin Res. Ed)* **316**, 17–20 (1998).
8. B. G. Birdwell, G. E. Raskob, T. L. Whitsett, S. S. Durica, P. C. Comp, J. N. George, T. L. Tytle, and P. A. McKee, "The clinical validity of normal compression ultrasonography in outpatients suspected of having deep venous thrombosis," *Ann. Intern Med.* **128**, 1–7 (1998).
9. J. C. de Valois, C. C. van Schaik, F. Verzijlbergen, B. van Ramshorst, B. C. Eikelboom, and O. J. Meuwissen, "Contrast venography: from gold standard to 'golden backup' in clinically suspected deep vein thrombosis," *Eur. J. Radiol.* **11**, 131–137 (1990).
10. A. W. A. Lensing, P. Prandoni, H. R. Buller, D. Casara, A. Cogo, and J. W. ten Cate, "Lower extremity venography with iohexol: results and complications," *Radiology* **177**, 503–505 (1990).
11. R. Taillefer, "Radiolabeled peptides in the detection of deep venous thrombosis," *Semin Nucl. Med.* **31**, 102–123 (2001).
12. B. Harmon, "Deep vein thrombosis: a perspective on anatomy and venographic analysis," *J. Thorac. Imaging* **4**, 15–19 (1989).
13. J. P. Kanne and T. A. Lalani, "Role of computed tomography and magnetic resonance imaging for deep venous thrombosis and pulmonary embolism," *Circulation* **109**, I-15–I-21 (2004).
14. F. C. Sampson, S. W. Goodacre, S. M. Thomas, and E. J. R. van Beek, "The accuracy of MRI in diagnosis of suspected deep vein thrombosis: systematic review and meta-analysis," *Eur. Radiol.* **17**, 175–181 (2007).
15. S. W. Goodacre, F. C. Sampson, M. Stevenson, A. Wailoo, A. Sutton, S. M. Thomas, T. Locker, and A. Ryan, "Measurement of the clinical and cost-effectiveness of non-invasive diagnostic testing strategies for deep vein thrombosis," *Health Technol. Assess (Rockv)* **10**, 1–228 (2006).
16. D. G. W. Fraser, A. R. Moody, P. S. Morgan, A. L. Martel, and I. Davidson, "Diagnosis of lower-limb deep venous thrombosis: a prospective blinded study of magnetic resonance direct thrombus imaging," *Ann. Intern Med.* **136**, 89–98 (2002).
17. "The diagnostic approach to acute venous thromboembolism," *Am. J. Respir. Crit. Care Med.* **160**, 1043–1066 (1999).

18. H. R. Buller, G. Agnelli, R. D. Hull, T. M. Hyers, M. H. Prins, and G. E. Raskob, "Antithrombotic therapy for venous thromboembolic disease: the seventh ACCP conference on antithrombotic and thrombolytic therapy," *Chest* **126**, 401S-428S (2004).

19. T. W. Wakefield, "Treatment options for venous thrombosis," *J. Vasc. Surg.* **31**, 613–620 (2000).

20. H. Xie, K. Kim, S. R. Aglyamov, S. Y. Emelianov, M. O'Donnell, W. F. Weitzel, S. K. Wrobleski, D. D. Myers, T. W. Wakefield, and J. M. Rubin, "Correspondence of ultrasound elasticity imaging to direct mechanical measurement in aging DVT in rats," *Ultrasound Med. Biol.* **31**, 1351–1359 (2005).

21. C. K. N. Patel and A. C. Tam, "Pulsed optoacoustic spectroscopy of condensed matter," *Rev. Mod. Phys.* **53**, 517–550 (1981).

22. A. C. Tam, "Application of photoacoustic sensing techniques," *Rev. Mod. Phys.* **58**, 381–431 (1986).

23. T. W. Wakefield, R. M. Strieter, C. A. Wilke, A. M. Kadell, S. K. Wrobleski, M. D. Burdick, R. Schmidt, S. L. Kunkel, and L. J. Greenfield, "Venous thrombosis-associated inflammation and attenuation with neutralizing antibodies to cytokines and adhesion molecules," *Arterioscler., Thromb., Vasc. Biol.* **15**, 258–268 (1995).

24. A. A. Oraevsky, A. A. Karabutov, S. V. Solomatin, E. V. Savateeva, V. G. Andreev, Z. Gatalica, H. Singh, and R. D. Fleming, "Laser optoacoustic imaging of breast cancer in vivo," *Proc. SPIE* **4256**, 6–15 (2001).

25. B. Pogue and M. Patterson, "Review of tissue simulating phantoms for optical spectroscopy, imaging and dosimetry," *J. Biomed. Opt.* **11**, 041102 (2006).

26. E. L. Madsen, J. A. Zagrebski, M. C. MacDonald, and G. R. Frank, "Ultrasound focal lesion detectability phantoms," *Am. J. Phys. Med.* **18**, 1171–1181 (1991).

27. A. Kharine, S. Manohar, R. Seeton, R. G. M. Kolkman, R. A. Bolt, W. Steenbergen, and F. F. M. de Mul, "Poly(vinyl alcohol) gels for use as tissue phantoms in photoacoustic mammography," *Phys. Med. Biol.* **48**, 357–370 (2003).

28. G. J. Diebold and T. Sun, "Properties of photoacoustic waves in one, two and three dimensions," *Acustica* **80**, 339–351 (1994).

29. A. B. Karpiouk, S. R. Aglyamov, S. Mallidi, W. G. Scott, J. M. Rubin, and E. Y. Emelianov, "Combined ultrasonic and photoacoustic imaging to age deep vein thrombosis: preliminary studies," *Proc.-IEEE Ultrason. Symp.* **1**, 399–402 (2005).

30. S. R. Aglyamov, A. R. Skovoroda, J. M. Rubin, M. O'Donnell, and S. Y. Emelianov, "Model-based reconstructive elasticity imaging of deep venous thrombosis," *IEEE Trans. Ultrason. Ferroelectr. Freq. Control* **51**, 521–531 (2004).

31. S. Prahl, "Tabulated molar extinction coefficient for hemoglobin in water," *Oregon Medical Laser Center*, see http://omlc.ogi.edu/spectra/hemoglobin/summary.html (2000).

32. W. F. Cheong, S. A. Prahl, and A. J. Welch, "A review of the optical properties of biological tissues," *IEEE J. Quantum Electron.* **26**, 2166–2185 (1990).

33. A. A. Oraevsky, E. V. Savateeva, S. V. Solomatin, A. A. Karabutov, V. G. Andreev, Z. Gatalica, T. Khamapirad, and P. M. Henrichs, "Optoacoustic imaging of blood for visualization and diagnostics of breast cancer," *Proc. SPIE* **4618**, 81–94 (2002).

34. N. Seyahi, A. Kahveci, M. R. Altiparmak, K. Serdengecti, and E. Erek, "Ultrasound imaging findings of femoral veins in patients with renal failure and its impact on vascular access," *Nephrol. Dial Transplant* **20**, 1864–1867 (2005).

35. J. M. Rubin, S. R. Aglyamov, T. W. Wakefield, M. O'Donnell, and S. Y. Emelianov, "Clinical application of sonographic elasticity imaging for aging of deep venous thrombosis: preliminary findings," *J. Ultrasound Med.* **22**, 443–448 (2003).

36. S. Y. Emelianov, S. R. Aglyamov, J. Shah, S. Sethuraman, W. G. Scott, R. Schmitt, M. Motamedi, A. Karpiouk, and A. Oraevsky, "Combined ultrasound, optoacoustic and elasticity imaging," *Proc. SPIE* **5320**, 101–112 (2004).